



HAL
open science

Water boiling at low pressure: dynamics of growth and bursting of bubbles in a plate-type evaporator

Patric Mantaropoulos, Florine Giraud, Brice Tremeac, Pascal Tobaly

► To cite this version:

Patric Mantaropoulos, Florine Giraud, Brice Tremeac, Pascal Tobaly. Water boiling at low pressure: dynamics of growth and bursting of bubbles in a plate-type evaporator. 14th IIR-Gustav Lorentzen Conference on Natural Refrigerants(GL2020), Dec 2020, Kyoto (on line), Japan. 10.18462/iir.gl.2020.1059 . hal-03106574

HAL Id: hal-03106574

<https://cnam.hal.science/hal-03106574>

Submitted on 11 Jan 2021

HAL is a multi-disciplinary open access archive for the deposit and dissemination of scientific research documents, whether they are published or not. The documents may come from teaching and research institutions in France or abroad, or from public or private research centers.

L'archive ouverte pluridisciplinaire **HAL**, est destinée au dépôt et à la diffusion de documents scientifiques de niveau recherche, publiés ou non, émanant des établissements d'enseignement et de recherche français ou étrangers, des laboratoires publics ou privés.

Water boiling at low pressure: dynamics of growth and bursting of bubbles in a plate-type evaporator

Patric MANTAROPOULOS, Florine GIRAUD, Brice TREMEAC, Pascal TOBALY

Laboratoire du Froid, des Systèmes Energétiques et Thermiques (Lafset), Cnam, HESAM Université, 292 rue Saint-Martin 75003 Paris, France, florine.giraud@lecnam.net

ABSTRACT

Water is a good candidate to be used as an eco-friendly refrigerant. However, its behaviour under sub-atmospheric pressure needs to be better understood to optimize the efficiency and sizing of compact evaporators. Previous studies conducted in a plate-type evaporator highlighted that after the bubbles burst, the formation and evaporation of a thin liquid film on the evaporator wall has a major contribution on heat transfer. This work thus aims to characterize the dynamics of vapour bubbles during nucleate boiling, and more specifically the projection height after the free surface breakup. Using previous high-speed visualizations, the bubbles' characteristics are computed thanks to an ad-hoc Python program. It is shown that the projection height is correlated with the growth velocity and the size of the bubble reached just before it bursts. The influence of relevant dimensionless numbers on the projection height is also studied to determine the underlying predominant forces.

Keywords: Refrigeration, Plate-type evaporators, Water, Bubbles, Low pressure, R-718.

1. INTRODUCTION

Many commonly used refrigerants are subject to restrictive standards due to their environmental impact. In the future, these restrictions are to be tightened. Alternatives must be found, and water could be one of them. However, using water in refrigeration installations requires to work at pressures close to the triple point (0.6 kPa). In these conditions, the hydrostatic pressure can no longer be neglected and thus induces an inhomogeneity in the boiling environment. In the case of a plate-type vertical evaporator, Giraud et al (2016) highlighted that most of the heat transfer during boiling is due to the vaporisation of a thin liquid film – formed by growth and bursting of vapour bubbles.

Boiling and bubble growth have been theorized for over a century. From the first modelling of a bubble's radius by Rayleigh (1917) to the developments of Plesset and Zwick (1954) and Forster and Zuber (1954) to the general model proposed by Mikic et al. (1970) and the simulations of Robinson and Judd (2004), among others, knowledge about bubbles behaviour in a variety of environments has not stopped extending. It is therefore well accepted that bubble growth is divided into three main regions, characterized by the phenomenon limiting the growth: the surface tension-, inertia- and diffusion- controlled growth regions. Yet, sub-atmospheric pressure boiling environments received little attention until now. Bubbles behave in a completely different way in these conditions: Van Stralen et al. (1975) brought to light that in pool boiling under sub-atmospheric pressure, bubbles grow mushroom-shaped and bigger than in atmospheric conditions. Most of the models developed in the past consider spherical or semi-spherical bubbles and do not consider the specificities of the boiling environment.

Thus, in order to study the parameters impacting the creation of the liquid film in a plate-type vertical evaporator, a characterization of the bubble growth and bursting dynamics based on previous experimental results is conducted. After a part dedicated to the presentation of the experimental bench, the data processing method is explained and the factors impacting the projection height of the droplets forming the liquid film are discussed.

2. EXPERIMENTAL BENCH

2.1. The evaporator

The main part of the bench is a plate-type vertical evaporator, illustrated in Fig.1. It is made up of three vertical plates, forming two channels in which circulate the primary and secondary fluid (water). The plates are made of stainless steel, except for the front one, which is made of PMMA to visualise the flow in the channel, as shown on Fig. 2. The separation plate thickness is 6mm.

On the refrigerant side, the thickness of the channel through which the refrigerant flows (the confinement thickness) can be set at 2, 4 or 6 mm (depending on the O-ring and spacer selected). The outer plate is transparent (PMMA), which allows boiling phenomena to be visualised by means of a high-speed camera (Phantom VEO410). Acquisitions are made at 3000 frames per second with a resolution of 1280 x 800 and an exposure time of 191.8 μ s.

The channel is fed from below by three 2 mm diameter tubes. The flow rate is set by means of a mass flow controller, which is controlled according to the desired liquid level in the evaporator. The water then leaves the evaporator as steam through a slit at its upper end.

The secondary fluid circulates in co-current at a flow rate of about 1 L/min. It enters the evaporator at the selected temperature by means of a thermostatic bath (set point between 11 and 28 °C). At the outlet, the measured temperature is between 10 and 21 °C. The channel thickness is set at 1 mm.

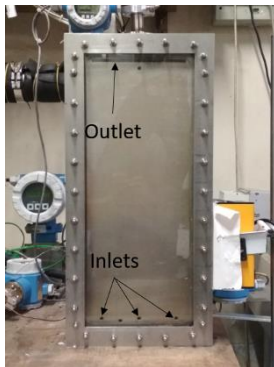


Figure 1: Photograph of the evaporator

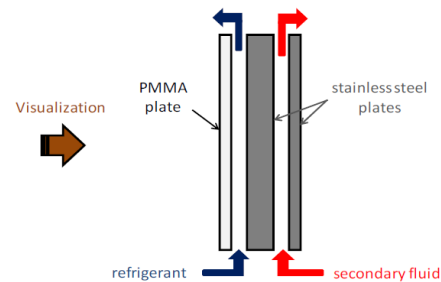


Figure 2: Scheme of the evaporator (from Giraud, 2016)

2.2. The bench

For the evaporator to operate continuously, the steam coming out of it is directed to a condenser. The condenser consists of a cylinder of 720 mm height and 300 mm inside diameter. A copper tubular exchanger (in which water circulates at a temperature imposed by a thermostatic bath) is placed in this container to condense the steam coming from the evaporator. This oversized exchanger allows the pressure to be imposed on the free surface in the evaporator. Thus, the experimental bench (Fig. 3) operates as a thermosiphon.



Figure 3: Photograph of the experimental bench

Once in a liquid state, the water leaves the condenser and flows in a recirculation pump to compensate for pressure drops. Finally, the liquid circulates through an expansion valve before the evaporator to enter the evaporator in a two-phase flow.

K-type thermocouples are placed at the inlet and outlet of each exchanger in the system, for both circuits (primary and secondary). Pressure sensors are also placed at each component and at the inlet and outlet of the expansion valve. The working pressures are between 0.7 and 1.7 kPa.

3. IMAGE PROCESSING

3.1. Contours detection

A test campaign previously carried out on this bench (Giraud and Tremeac, 2019) enabled video recordings of the bubbles formed in the evaporator, captured by the high-speed camera, thus making it possible to study their growth and bursting. To clear and analyse the captured videos, an image processing program was developed in Python language, part of the recordings could thus be analysed automatically.

This is done by cutting each video into a sequence of images. The images are then processed in such a way as to isolate the bubble: the background of the image is replaced by a black background, while the contours of the bubble are detected and traced in white (see Fig. 4, bottom). This process is made possible by the OpenCV for Python module.

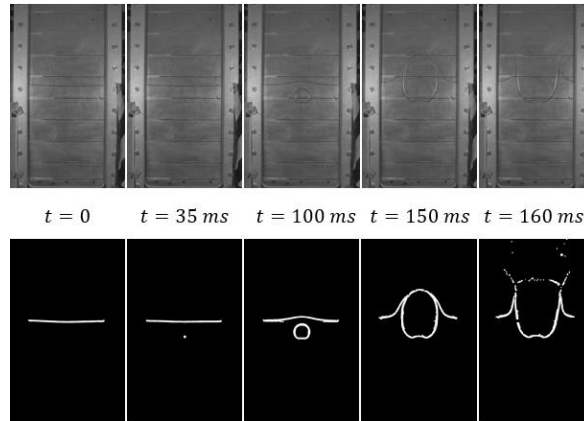


Figure 4: Example of image processing (top: raw, bottom: processed)

3.2. Measurements

This pre-processing allows to compute the relevant characteristics of the bubbles' evolution. This study focuses on the very last instant of growth, before the bubble bursts: the parameters described below are therefore at their maximum, hence the index *max*. The apparent area, which informs about the size of the bubble, is computed as follows: for each column of pixels, the chord length of the bubble is computed by subtracting the coordinates of the ends of the bubble. The sum of all the chords gives the bubble's apparent area in pixels. The value is then converted in square meters. The equivalent radius is calculated as the radius of the circle with the same apparent area(see Eq. (1)).

$$R_{max}^{eq} = \sqrt{\frac{S_{max}}{\pi}} \quad \text{Eq. (1)}$$

Another important characteristic of the bubble growth is its growth velocity. The derivative of the apparent area with respect to time is the most direct way of describing the expansion of the bubble. It will then be referred to as the *expansion velocity* U_f , and its expression is detailed in Eq. (2).

$$U_f = \left(\frac{dS}{dt}\right)_{t=t_{bursting}} \quad \text{Eq. (2)}$$

Finally, the projection height H_p may be related to the deposited liquid film (see Fig. 6a). Indeed, during the evolution of the bubble, the wall of the channel is wetted by liquid displacement during growth, then by projection and droplet deposition after bursting. The projection height then corresponds to the maximum height of the liquid film. In this work, it is defined as follows: at each instant after the burst, the maximum pixel density of the image is calculated. That is, for each image, the number of white pixels above the free surface is counted line by line. The altitude of the line containing the most pixels corresponds to a height in pixels, the reference being the bottom of the image. The difference between this height and the liquid level H_r is used as the projection height. Figure 6b illustrates this definition.

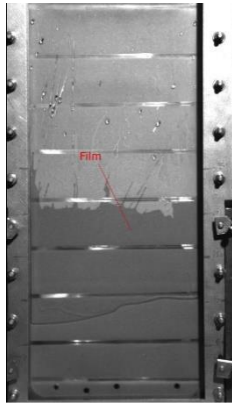


Figure 6a: Illustration of the liquid film

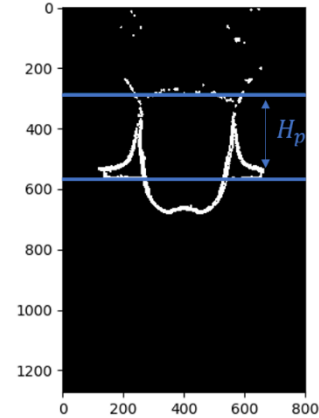


Figure 6b: calculation of the projection height (pixels)

Although the contours detected by the program are probably those in contact with the PMMA plate, we will assume in this study that the calculated projection height and apparent area are close to those in contact with the stainless steel plate.

4. RESULTS AND DISCUSSION

4.1. Qualitative analysis

The processing of 146 exploitable videos enabled a preliminary qualitative analysis. Without considering the properties of the fluid, focusing on the bubble's dynamics and size, it appears that the projection height is linked to the state of the bubble before the free surface breaks up. Indeed, as illustrated on Fig. 7, the projection height is correlated to the maximum apparent area of the bubble at the time of burst and to its maximum expansion velocity at that same instant.

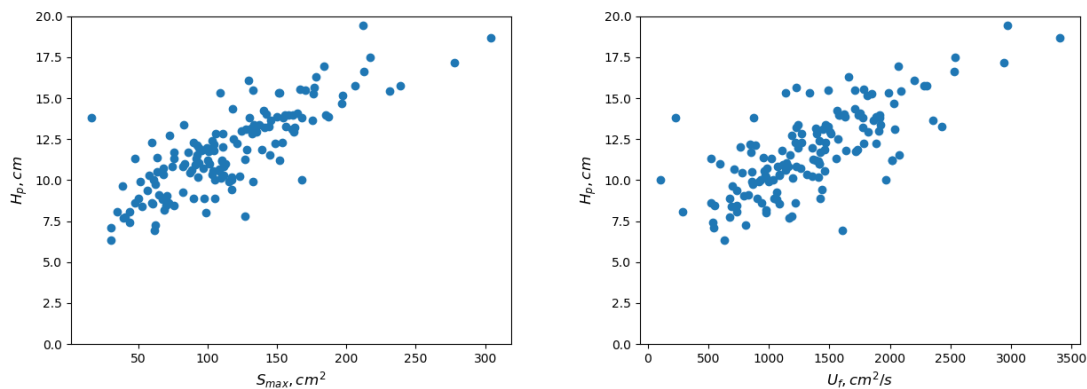


Figure 7: Projection height versus apparent area before bursting (left) and projection height versus expansion velocity (right)

In other words, the bigger the apparent area before bursting, the higher the projection. Likewise, the faster the growth at the time of free surface breakup, the higher the projection. This can be explained by the fact that the interface between the bubble and the liquid - which merges with the free interface at the time of bursting - turns into droplets at the time of rupture. The kinetic energy acquired by the interface during bubble's growth is then transmitted to the droplets.

This first insight into the influence of a bubble's size and velocity on the projection height can be further developed by integrating the thermo-physical properties of the working fluid and considering the different forces acting on the bubble at the time of bursting.

4.2. Forces and dimensionless numbers

During a bubble's growth, the predominance of certain forces over others determines its characteristics (size, shape, velocity...). In the present study, liquid inertia is compared to surface tension and viscous dissipation, as these forces seem to play a significant role in the bubble's evolution. For that purpose, dimensionless numbers are defined and their impact over projection height is investigated.

Weber number, defined in eq. (3), is used to evaluate the balance between inertia and surface tension. The characteristic velocity (v_{max}^+) corresponds to the velocity of the interface between the liquid and the bubble at its highest point, at the time of burst.

$$We = \frac{\rho_L v_{max}^+{}^2 R_{max}^{eq}}{\sigma} \quad \text{Eq. (3)}$$

ρ_L and σ are respectively the density and surface tension of the liquid.

The values of We range between 10^2 and 10^4 . Since this number represents the ratio between inertia and surface tension, it appears that inertia is predominant in comparison with surface tension: the kinetic energy accumulated during growth surpasses the surface tension that keeps the free surface whole. Consequently, the free surface breaks.

On the other hand, the balance between inertia and viscous forces is commonly evaluated by Reynolds number. A modified Reynolds number (Re_b) is therefore used for that purpose and defined in eq. (4). Like the previous result, it seems that liquid inertia predominates over viscous dissipation: Re_b ranges between 10^4 and 10^5 . Thus, at the time of burst, viscous dissipation in the liquid is negligible.

$$Re_b = \frac{\rho_L v_{max}^+ R_{max}^{eq}}{\mu_L} \quad \text{Eq. (4)}$$

Fig. 8 shows the influence of We and Re_b on projection height. The projection height seems correlated to the Weber number: the greater the liquid's kinetic energy at the time of burst compared to surface tension, the higher the projection. In other words, the more "remaining" energy after the free-surface breakup, the more energy transferred to the droplets. Likewise, the projection height is correlated to the modified Reynolds number: the energy transferred to the droplets depends on the amount of energy transferred to the liquid by viscous dissipation (the less energy dissipated by viscosity, the more energy transferred to the droplets).

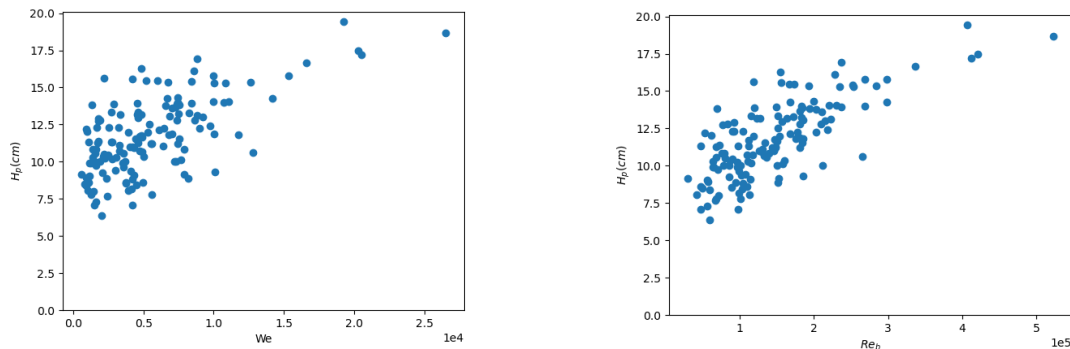


Figure 8: Projection height versus We (left) and versus Re_b (right)

5. CONCLUSIONS

Video recordings of growth and bursting of water bubbles have been processed and analysed. In a sub-atmospheric pressure and narrow environment, the characteristics of the bubbles have been measured, amongst which the projection height, the apparent area and the expansion velocity. It has been brought to light that the projection height is correlated to the expansion velocity and the apparent area. Moreover, dimensionless numbers have been used to consider the force balance at the time of burst: the projection height seems to be also correlated with these numbers. In conclusion, the liquid's kinetic energy at the time of burst seems to have a major impact on the formation of the thin liquid film by projecting droplets on the exchanger wall.

ACKNOWLEDGEMENTS

The authors are grateful to L. Fluro for performing the experimental measurements.

NOMENCLATURE

R_{max}^{eq}	equivalent radius (m)	v_{max}^+	upper interface velocity ($m \times s^{-1}$)
S_{max}	apparent area (m^2)	ρ_L	density of the liquid ($kg \times m^{-3}$)
U_f	expansion velocity (m^2/s)	μ_L	viscosity of the liquid ($Pa \times s$)
H_p	projection height (cm)	σ	surface tension of the liquid ($N \times m^{-1}$)

REFERENCES

- Forster, H.K., Zuber, N., 1954. Growth of a Vapor Bubble in a Superheated Liquid. *Journal of Applied Physics* 25, 474–478. <https://doi.org/10.1063/1.1721664>
- Giraud, F., Toublanc, C., Rullière, R., Bonjour, J., Clause, M., 2016. Experimental study of water vaporization occurring inside a channel of a smooth plate-type heat exchanger at subatmospheric pressure. *Applied Thermal Engineering* 106, 180–191. <https://doi.org/10.1016/j.applthermaleng.2016.05.151>
- Giraud, F., Tremeac, B., 2019. Influences of confinement on subatmospheric water vaporization phenomena in a vertical rectangular channel. *International Journal of Heat and Mass Transfer* 145, 118725. <https://doi.org/10.1016/j.ijheatmasstransfer.2019.118725>
- Lord Rayleigh, 1917. VIII. On the pressure developed in a liquid during the collapse of a spherical cavity. *The London, Edinburgh, and Dublin Philosophical Magazine and Journal of Science* 34, 94–98. <https://doi.org/10.1080/14786440808635681>
- Michaie, S., Rullière, R., Bonjour, J., 2019. Towards a more generalized understanding of pool boiling at low pressure: Bubble dynamics for two fluids in states of thermodynamic similarity. *Experimental Thermal and Fluid Science* 101, 217–230. <https://doi.org/10.1016/j.expthermflusci.2018.10.009>
- Mikic, B.B., Rohsenow, W.M., Griffith, P., 1970. On bubble growth rates. *International Journal of Heat and Mass Transfer* 13, 657–666. [https://doi.org/10.1016/0017-9310\(70\)90040-2](https://doi.org/10.1016/0017-9310(70)90040-2)
- Plesset, M.S., Zwick, S.A., 1954. The Growth of Vapor Bubbles in Superheated Liquids. *Journal of Applied Physics* 25, 493–450.
- Robinson, A.J., Judd, R.L., 2004. The dynamics of spherical bubble growth. *International Journal of Heat and Mass Transfer* 47, 5101–5113. <https://doi.org/10.1016/j.ijheatmasstransfer.2004.05.023>
- van Stralen, S.J.D., Cole, R., Sluyter, W.M., Sohal, M.S., 1975. Bubble growth rates in nucleate boiling of water at subatmospheric pressures. *International Journal of Heat and Mass Transfer* 18, 655–669. [https://doi.org/10.1016/0017-9310\(75\)90277-X](https://doi.org/10.1016/0017-9310(75)90277-X)